JMB

Available online at www.sciencedirect.com

ScienceDirect

ELSEVIER

Structural Basis for Catalysis by Onconase

J. Eugene Lee[1]†, Euiyoung Bae[1,2]†, Craig A. Bingman[2] George N. Phillips Jr[1,2]* and Ronald T. Raines[1,3]*

[1]*Department of Biochemistry University of Wisconsin-Madison, Madison WI 53706-1544, USA*

[2]*Center for Eukaryotic Structural Genomics University of Wisconsin-Madison, Madison Wisconsin 53706-1544, USA*

[3]*Department of Chemistry University of Wisconsin-Madison, Madison WI 53706-1322, USA*

Onconase® (ONC) is a homolog of bovine pancreatic ribonuclease (RNase A) from the frog *Rana pipiens*. ONC displays antitumoral activity and is in advanced clinical trials for the treatment of cancer. Here, we report the first atomic structures of ONC–nucleic acid complexes: a T89N/E91A ONC–5′-AMP complex at 1.65 Å resolution and a wild-type ONC–d(AUGA) complex at 1.90 Å resolution. The latter structure and site-directed mutagenesis were used to reveal the atomic basis for substrate recognition and turnover by ONC. The residues in ONC that are proximal to the scissile phosphodiester bond (His10, Lys31, and His97) and uracil nucleobase (Thr35, Asp67, and Phe98) are conserved from RNase A and serve to generate a similar bell-shaped pH *versus* k_{cat}/K_M profile for RNA cleavage. Glu91 of ONC forms two hydrogen bonds with the guanine nucleobase in d(AUGA), and Thr89 is in close proximity to that nucleobase. Installing a neutral or cationic residue at position 91 or an asparagine residue at position 89 virtually eliminated the 10^2-fold guanine:adenine preference of ONC. A variant that combined such substitutions, T89N/E91A ONC, actually preferred adenine over guanine. In contrast, installing an arginine residue at position 91 increased the guanine preference and afforded an ONC variant with the highest known k_{cat}/K_M value. These data indicate that ONC discriminates between guanine and adenine by using Coulombic interactions and a network of hydrogen bonds. The structure of the ONC–d(AUGA) complex was also used to probe other aspects of catalysis. For example, the T5R substitution, designed to create a favorable Coulombic interaction between ONC and a phosphoryl group in RNA, increased ribonucleolytic activity by twofold. No variant, however, was more toxic to human cancer cells than wild-type ONC. Together, these findings provide a cynosure for understanding catalysis of RNA cleavage in a system of high medicinal relevance.

© 2007 Elsevier Ltd. All rights reserved.

Keywords: cytotoxin; ribonuclease; RNA; substrate specificity; X-ray crystallography

Edited by J. Doudna

*Corresponding authors. E-mail addresses: phillips@biochem.wisc.edu; raines@biochem.wisc.edu. † J.E.L. and E.B. contributed equally to this work.

Introduction

The viability of organisms relies on the ability of proteins to recognize nucleic acids. In contrast, the ability of an enzyme to both recognize a nucleic acid and catalyze its cleavage can have deleterious consequences. For example, ribonucleases can be cytotoxic because cleaving RNA renders indecipherable its encoded information.[1,2]

Onconase® (ONC; Figure 1(a)) is a ribonuclease found in the eggs and early embryos of the frog *Rana pipiens*. ONC is a homolog of bovine pancreatic ribonuclease (RNase A),[3] and the two proteins share 30% amino acid sequence identity and a similar three-dimensional structure.[4] ONC is in confirma-
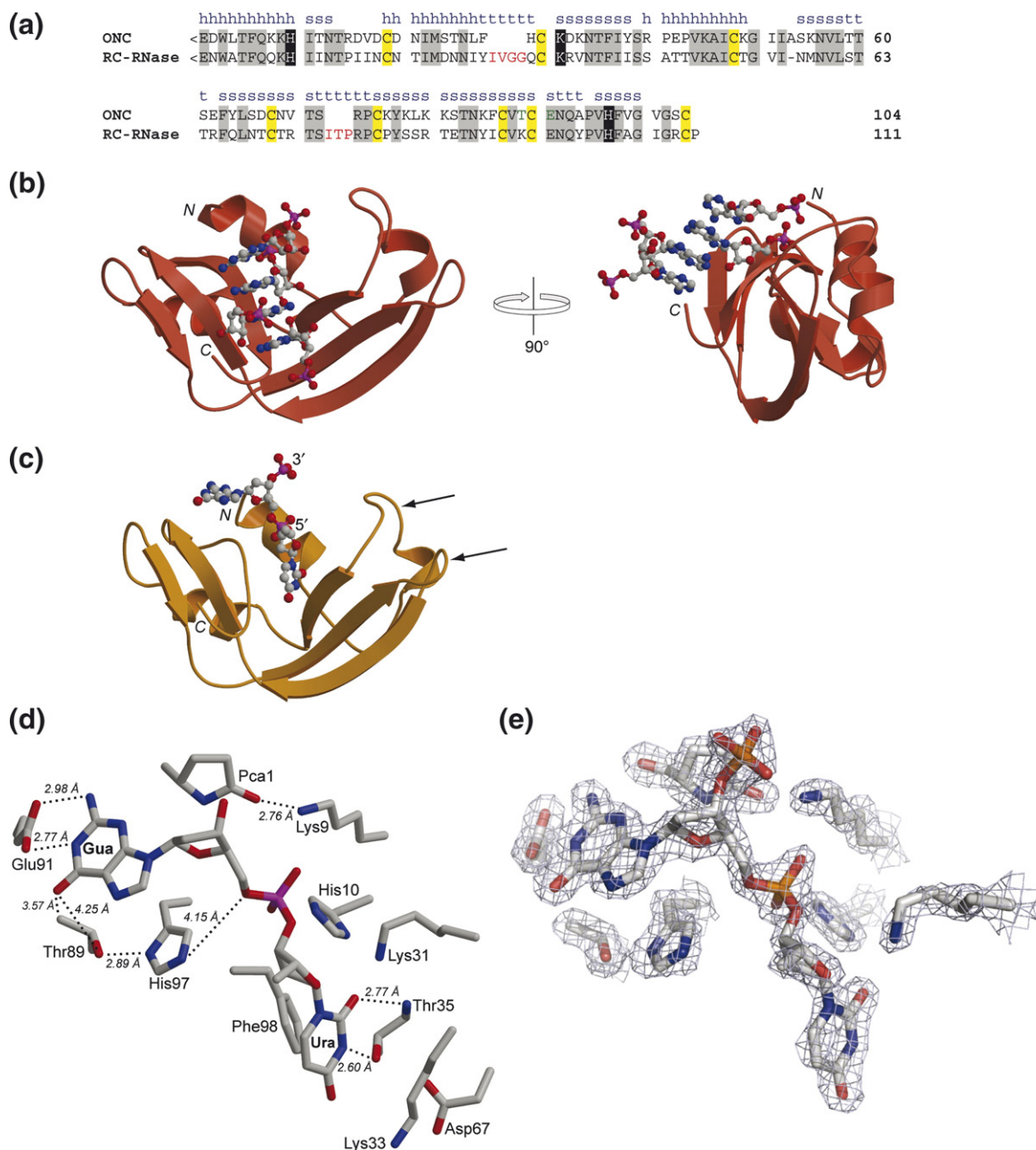
Figure 1. Primary and tertiary structure of ONC. (a) Amino acid sequence alignment of ONC and RC-RNase. The secondary structure of ONC is labeled as h (α-helix), s (β-strand), or t (turn). Residues conserved between the two ribonucleases are in gray boxes. <E denotes a pyroglutamate residue. Key active-site residues are in black boxes. Cysteine residues that form intramolecular disulfide bonds are in yellow boxes. Residues that participate in the nucleobase recognition at the B_2 subsite in ONC are in green. Extra amino acid residues in the loops of RC-RNase are in red. (b) A ribbon diagram of the three-dimensional structure of the T89N/E91A ONC–5′-AMP complex (PDB entry 2GMK). (c) A ribbon diagram of the three-dimensional structure of the ONC–d(AUGA) complex (PDB entry 2I5S). The two flanking adenosine nucleotides are not included in the diagram because of their low electron density. The two arrowheads indicate the two loops that were subjected to elongation. (d) A stick diagram of the active site and B_1 and B_2 subsites in the ONC–d(AUGA) complex. Thr35 forms two hydrogen bonds with the uracil nucleobase. Glu91 forms two hydrogen bonds with the guanine nucleobase. Thr89 is located close to the carbonyl oxygen of guanine. (e) Electron density map of the active site (σ-weighted $2F_o$–F_c) contoured at 1.5σ over background. Images in (b)–(e) were created with the program MOLSCRIPT and rendered with the program Raster3D.[79]

tory phase IIIb clinical trials for the treatment of malignant mesothelioma,[5,6] and has been granted both orphan drug and fast track status by the US Food and Drug Administration. ONC also inhibits human immunodeficiency virus type 1 replication.[7]

ONC is a unique ribonuclease. The protein exhibits remarkable conformational stability (T_m = 90 °C).[8] Four disulfide bonds and the absence of a *cis*-prolyl peptide bond contribute to this attribute.[8–11] ONC evades the cellular ribonuclease

inhibitor protein (RI),[12] to which other ribonucleases bind with femtomolar affinity.[13–19] The exceptional conformational stability and the RI-evading ability contribute to its cytotoxic activity.[8,17,20]

ONC is a poor catalyst. The ribonucleolytic activity of ONC is three to five orders of magnitude lower than that of RNase A due, in large part, to low affinity for its substrate.[21] Nonetheless, the catalytic activity of ONC is necessary for cytotoxicity.[22]

Homologs of RNase A bind a pyrimidine residue on the 5′ side of the scissile phosphodiester bond in a small, conserved nucleobase-binding site.[23–26] ONC displays a distinct preference for a guanosine nucleoside on the 3′ side of the scissile phosphodiester bond.[21] This guanine preference is found for other frog ribonucleases,[27] but not in mammalian homologs.[28] The basis for this guanine preference in ONC is unknown. tRNA appears to be the major cellular substrate for ONC.[29] A recent study revealed an unconventional cleavage sequence for ONC: the guanosine–guanosine phosphodiester bond in the variable loop or the D-arm in tRNA.[30]

Here, we report the first crystal structures of ONC–nucleic acid complexes. We use this structural information to address key issues in ONC catalysis. First, we determine the molecular basis for the nucleobase specificity of ONC through a systematic site-directed mutagenesis study. Next, we ask whether the low level of catalytic activity of ONC can be enhanced by a rational design approach. Finally, we seek to confirm the cellular target sequence of ONC *in vitro* using two novel fluorogenic substrates. We anticipate that the development of ONC as a cancer chemotherapeutic will benefit from the incipient understanding of its catalysis.

Results

Structural overview

The crystalline structures of the T89N/E91A ONC–5′-AMP and ONC–d(AUGA) complexes were solved to a resolution of 1.65 Å and 1.90 Å, respectively. Data collection, refinement, and model statistics are summarized in Table 1. The electron density was continuous for main-chain and side-chain atoms. Asymmetric units of the structures contain a single monomer with a chain-fold virtually identical with that of free ONC (Protein Data Bank (PDB) entry 1ONC).[4] Both structures exhibit the typical bilobal shape of the RNase A superfamily, with two anti-parallel β-sheets flanked by two α-helices. In addition, our structures contain the rare N-terminal pyroglutamate residue and C-terminal disulfide bond, which are conserved among the amphibian members of the superfamily.

Structure of the T89N/E91A ONC–5′-AMP complex

In the crystalline T89N/E91A ONC–5′-AMP complex, four 5′-AMP molecules are bound to each

Table 1. Summary of data collection and refinement statistics

	T89N/E91A ONC–5′-AMP	Wild-type ONC–d(AUGA)
A. *Data collection*		
Space group	$P2_12_12_1$	$P2_12_12$
Unit cell parameters		
a (Å)	29.0	129.2
b (Å)	52.1	26.1
c (Å)	66.1	32.5
Data collection statistics		
Resolution range (Å)	66.14–1.65	64.62–1.90
	(1.70–1.65)	(1.95–1.90)
No. reflections measured/	336,231	91,217
No. reflections unique	12,645	9270
Completeness (%)	99.9 (99.6)	99.7 (95.9)
R_{merge}[a]	0.054 (0.663)	0.125 (0.517)
Redundancy	26.6 (5.1)	9.8 (3.3)
Mean σ/I	40.66 (3.32)	12.30 (2.52)
B. *Refinement statistics*		
Resolution range (Å)	40.93–1.65	32.49–1.90
No. reflections	12,597	9229
R_{cryst}[b]	0.165	0.178
R_{free}[c]	0.217	0.240
RMSD from ideal		
Bond lengths (Å)	0.010	0.013
Bond angles (deg.)	1.718	1.415
Average B-factor (Å^2)	19.35	16.60
Number of water molecules	196	155
Ramachandran plot		
Favored regions (%)	98.1	100.0
Allowed regions (%)	1.9	0.0

Values in parentheses are for the highest-resolution shell.
[a] $R_{merge} = \Sigma_k \Sigma_i |I_i(h) - \langle I(h) \rangle| / \Sigma_h \Sigma_i I_i(h)$, where $I_i(h)$ is the intensity of an individual measurement of the reflection and $<I(h)>$ is the mean intensity of the reflection.
[b] $R_{cryst} = \Sigma_h ||F_{obs}| - |F_{calc}|| / \Sigma_h |F_{obs}|$, where F_{obs} and F_{calc} are the observed and calculated structure factor amplitudes, respectively.
[c] R_{free} was calculated as R_{cryst} using 5.0% of the randomly selected unique reflections that were omitted from structure refinement.

enzyme molecule in a non-productive mode (Figure 1(b)). The nucleobases of the 5′-AMP molecules form a stack that makes contact with multiple enzyme molecules in the crystal lattice. One of the four 5′-AMP molecules has its 5′-phosphate group bound in the active site of the enzyme. Another 5′-AMP molecule is located at the interface between two enzyme molecules. The remaining two 5′-AMP molecules show no significant interaction with the enzyme and have relatively high B-factors.

Structure of the wild-type ONC–d(AUGA) complex

In the crystalline ONC–d(AUGA) complex, one nucleic acid molecule is bound to one enzyme molecule (Figure 1(c)). There was no electron density above the noise level for the 3′ adenosine. The electron density for the 5′ adenosine was less than that of a typical water molecule, and was not included in the model. The disorder in these two flanking nucleosides suggests that they do not interact significantly with the enzyme.

The conformation of the Glu91 and His97 side-chains in the ONC–d(AUGA) complex differed dramatically from those in free ONC (PDB entry 1ONC).[4] The χ_2 dihedral angle of His97 was investigated in detail and the residue was assigned to a conformation that had the most uniform B-value around the imidazole ring. This conformation, in which $N^{\delta 1}$ forms a 2.89 Å hydrogen bond with $O^{\gamma 1}$ of Thr89 (Figure 1(d) and (e)), is the one supported best by the diffraction data. The alternative conformation, which puts $N^{\delta 1}$ close to $O^{5\prime}$ of guanosine, had refined B-factors around the imidazole ring that varied by nearly twofold, with the B-factors for the nitrogen atoms being too large and those of the carbon atoms being too small relative to the surrounding residues.

Effect of pH on catalysis

RNase A cleaves RNA molecules by concerted general acid–base catalysis using the active-site residues His12 and His119.[31–34] In this mechanism, both a protonated and an unprotonated histidine residue are required for efficient catalysis. As a result, the pH *versus* k_{cat}/K_M profile of RNase A is a classic bell-shaped curve with a maximal catalytic activity near pH 6.[35,36] These histidine residues are conserved in ONC and other amphibian homologs, suggesting that the catalytic mechanism of RNase A could be operative within the amphibian subfamily (Figure 2). A recent study by Liao and co-workers showed, however, that the pK_a values of the catalytic histidine residues in RC-RNase 3, an amphibian homolog from the bullfrog (*Rana catesbeiana*), were significantly lower (4.26 and 5.96) than those manifested in RNase A.[37] Because of these low pK_a values, the catalytic activity of RC-RNase 3 is maximal near pH 5.[38]

To ensure that assays of the enzymatic activity of ONC were performed at an optimal pH, values of k_{cat}/K_M for the cleavage of, 6-carboxyfluorescein (6-FAM)–dArUdGdA–6-carboxytetramethylrhodamine (6-TAMRA) by ONC were determined in buffers of various pH values. The pH *versus* k_{cat}/K_M profile for ONC has a symmetric bell shape with pK_a values of 5.84 ± 0.05 and 6.77 ± 0.04 (Figure 3), which are similar to those of RNase A.[39–41] Accordingly, assays were performed in a buffer of pH 6.0, which enables
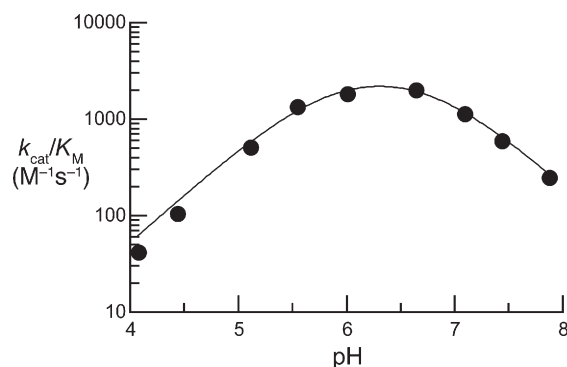
Figure 3. pH *versus* k_{cat}/K_M profile for the cleavage of 6-FAM–dArUdGdA–6-TAMRA by ONC. Assays were performed at 23 °C in 1.0 mM buffer, 1.0 M NaCl. Determination of k_{cat}/K_M values was performed in triplicate. Data were fit to equation (1) by non-linear least-squares regression analysis to give pK_a values of 5.84 ± 0.05 and 6.77 ± 0.04.

nearly maximal activity and allows for direct comparison with data for RNase A.

Residues in the B_1 subsite

RNase A and its homologs bind to RNA substrates in a cleft, leading to interactions that extend beyond the scissile bond. In RNase A, two subsites for a nucleobase (B_1 and B_2)[25,26,42,43] and four subsites for a phosphoryl group (P_{-1}, P_0, P_1, and P_2)[44–46] have been characterized in detail.[3] The enzyme catalyzes the cleavage of the P–O$^{5\prime}$ bond of a substrate bound in the B_1–P_1–B_2 subsites.

In the structure of the ONC–d(AUGA) complex, several residues of ONC are in close contact with the nucleobase moieties of d(AUGA). Lys33, Thr35, Asp67, and Phe98 are proximal to the uracil nucleobase (Figure 1(d)). $O^{\gamma 1}$ and the backbone amide nitrogen atom of Thr35 form two hydrogen bonds with N_4 and O_2, respectively, of that nucleobase. The distance between N^{ζ} of Lys 33 and O^4 of the uracil base is 3.73 Å. $O^{\delta 1}$ of Asp67 forms a hydrogen bond with $O^{\gamma 1}$ of Thr35. Each of these residues, except Lys33, is conserved in the RNase A superfamily, and hence constitute the B_1 subsite in ONC.

Residues in the B_2 subsite

In the structure of crystalline ONC–d(AUGA) complex, Glu91 forms two hydrogen bonds with the guanine nucleobase of d(AUGA) (Figure 1(d)), and Thr89 is located in close proximity to this nucleobase. We hypothesized that these two residues constitute the B_2 subsite of ONC, where B_2 refers to the nucleobase on the 3′ side of the scissile bond. To reveal the molecular basis for the guanine preference, we used site-directed mutagenesis to replace Thr89 and Glu91 with residues that differ in their net charge and ability to form hydrogen bonds (Table 2), and determined whether these variants showed an altered nucleobase preference.
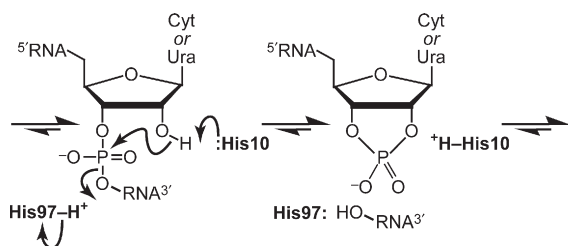

Figure 2. Putative mechanism of catalysis of RNA cleavage by ONC. In this transphosphorylation reaction, His10 acts as a base, and His97 acts as an acid.

Variants with an increased preference for guanine

Insertion of a positive charge at position 89 increased the guanine preference of ONC for cleavage of 6-carboxyfluorescein–dArUdGdA–6-carboxytetramethylrhodamine (UpG) relative to 6-carboxyfluorescein–dArUdAdA–6-carboxytetra-methylrhodamine (UpA) by tenfold (Figure 4; Table 2). The T89R and T89K variants displayed a 10^3-fold preference for guanine over adenine. Furthermore, the value of k_{cat}/K_M for the cleavage of a guanine-containing substrate (UpG) by T89R ONC was increased by threefold from that of the wild-type enzyme.

Variants with a decreased preference for guanine

Elimination of the negative charge at position 91 diminished the preference of ONC for guanine over adenine, and increased the value of k_{cat}/K_M for the cleavage of an adenine-containing substrate (UpA, Table 2). The E91A, E91Q, and E91N variants of ONC cleaved UpG two- to ninefold more quickly than UpA, indicative of substantially lower preference for guanine than that of the wild-type enzyme. The largest change in preference was observed with E91K ONC, which actually had a 1.6-fold preference for UpA over UpG. Each of these variants had three- to tenfold greater UpA-cleaving activity than did the wild-type enzyme.

Replacing Thr89 with an asparagine residue increased the value of k_{cat}/K_M for UpA cleavage by threefold (Table 2). In addition, the T89N substitution decreased the guanine preference of ONC by 50-fold. An aspartate or glutamine residue
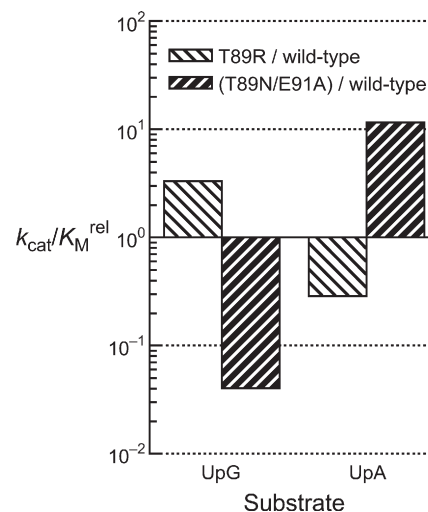

Figure 4. Effect of Thr89 and Glu91 on the substrate specificity of ONC. Bars indicate the effect of replacing Thr89 or Glu91 on the value of k_{cat}/K_M for the cleavage of 6-FAM–dArUdGdA–6-TAMRA (UpG) and 6-FAM–dArUdAdA–6-TAMRA (UpA). The guanine:adenine preference of T89R ONC is 3.3×10^3-fold greater than that of T89N/E91A ONC (Table 2).

at this position likewise decreased the guanine preference, though without increasing the k_{cat}/K_M value. Combining the T89N and E91A substitutions augmented their individual effect. T89N/E91A ONC had the highest catalytic activity toward UpA among all of the variants, with a greater than 12-fold increase from the wild-type enzyme (Figure 4; Table 2). Moreover, T89N/E91A ONC had a com-

Table 2. Values of k_{cat}/K_M, m/z, and IC$_{50}$ for ONC and its variants

ONC	k_{cat}/K_M			m/z[a]		IC$_{50}$ (μM)[c]
	UpG ($M^{-1}s^{-1}$)[b]	UpA ($M^{-1}s^{-1}$)[b]	UpG/UpA	Expected	Observed	
Wild-type	$4.2(\pm0.5)\times10^4$	$3.8(\pm0.2)\times10^2$	1.1×10^2	11,820	11,820	0.2
T89A	$1.5(\pm0.1)\times10^4$	$4.7(\pm0.4)\times10^2$	32	11,790	11,793	0.4
T89K	$4.1(\pm0.3)\times10^4$	$7.0(\pm0.4)\times10^1$	5.9×10^2	11,820	11,824	1.0
T89R	$1.4(\pm0.1)\times10^5$	$1.1(\pm0.1)\times10^2$	1.3×10^3	11,875	11,868	0.8
T89D	$1.2(\pm0.1)\times10^3$	$1.1(\pm0.1)\times10^2$	11	11,834	11,840	2.0
T89Q	$1.4(\pm0.1)\times10^3$	$3.5(\pm0.2)\times10^1$	40	11,847	11,852	ND
T89N	$2.6(\pm0.2)\times10^3$	$1.2(\pm0.1)\times10^3$	2.2	11,833	11,826	0.7
E91A	$3.9(\pm0.3)\times10^3$	$1.6(\pm0.1)\times10^3$	2.4	11,762	11,750	1.5
E91Q	$9.4(\pm0.3)\times10^3$	$1.1(\pm0.1)\times10^3$	8.6	11,819	11,827	0.6
E91N	$4.2(\pm0.3)\times10^3$	$1.6(\pm0.3)\times10^3$	2.6	11,811	11,805	ND
E91K	$2.4(\pm0.1)\times10^3$	$3.8(\pm0.3)\times10^3$	0.63	11,819	11,828	ND
T89N/E91A	$1.7(\pm0.3)\times10^3$	$4.4(\pm0.2)\times10^3$	0.39	11,775	11,780	2.5
T89K/E91A	$7.5(\pm0.3)\times10^3$	$5.6(\pm0.2)\times10^2$	13	11,788	11,793	1.7
T5K	$5.8(\pm0.1)\times10^4$	ND[d]	ND	11,846	11,852	0.4
T5R	$8.3(\pm0.5)\times10^4$	ND	ND	11,874	11,881	1.2
K33V	$4.4(\pm0.3)\times10^4$	$3.7(\pm0.3)\times10^2$	1.2×10^2	11,791	11,795	ND
K33V/T89K	$7.1(\pm0.7)\times10^4$	$1.6(\pm0.2)\times10^2$	4.4×10^2	11,818	11,823	ND
IVGGITP	$1.9(\pm0.2)\times10^4$	$5.3(\pm0.4)\times10^2$	36	12,447	12,454	4.0
L27I/F28Y IVGGITP	$3.4(\pm0.2)\times10^4$	$6.0(\pm0.2)\times10^2$	57	12,463	12,470	4.0

[a] Values of m/z were determined by matrix-assisted laser desorption/ionization–time-of-flight mass spectrometry.
[b] Values of k_{cat}/K_M ($\pm$SE) are for cleavage of 6-FAM–dArUdGdA–6-TAMRA or 6-FAM–dArUdAdA–6-TAMRA in 0.10 M Mes–NaOH (pH 6.0), 0.10 M NaCl at 23($\pm$2) °C.
[c] Values of IC$_{50}$ ($\pm$SE) are for incorporation of [*methyl*-^{3}H]thymidine into the DNA of K-562 cells exposed to ONC or a variant, and were calculated with equation (3).
[d] ND, not determined.

plete shift in nucleobase preference, favoring adenine over guanine by 2.6-fold.

Inhibition of catalysis

Catalysis of 6-FAM–dArUdGdA–6-TAMRA cleavage by wild-type ONC and its variants was inhibited by the nucleotides 5′-GMP and 5′-AMP (Table 3). Wild-type ONC was inhibited by 5′-GMP and 5′-AMP with K_i values of $6.7(\pm 0.5) \times 10^2$ μM and $3.7(\pm 0.3) \times 10^3$ μM, respectively. The K_i values of the T89K and T89R variants, which manifested an increased preference for the guanine nucleobase, did not differ markedly from that of wild-type ONC. On the contrary, variants with a decreased guanine preference showed relatively large changes in K_i values. Inhibition by 5′-AMP was threefold and sixfold more pronounced for T89N ONC and T89N/E91A ONC, respectively. Inhibition by 5′-GMP was twofold less pronounced for E91A ONC.

Rational design of ONC variants with enhanced catalytic activity

Previous structural investigations have shown that the structure of ONC is less flexible than that of other ribonucleases.[26,47] This rigidity could hinder facile interaction with the substrate. The structure of the ONC–d(AUGA) complex supports this hypothesis. The RMSD of the backbone C^α of ONC in the free and complexed form is just 0.4 Å,[48] suggesting little conformational change upon substrate binding.

Global approach

We sought to increase the catalytic activity of ONC by enhancing its flexibility. Sica and co-workers have implicated the short loops of ONC as causing rigidity.[49] Amphibian ribonucleases are grouped into two subfamilies.[50] The members of the subfamily with two short loops connecting the α2 helix and the β2 strand, and the β4 and β5 strands (ONC, RC-RNase 2, RC-RNase 4, and RC-RNase 6) have a low level of catalytic activity.[38,51,52] The second subfamily, represented by RC-RNase and RC-RNase L1, contain loops with additional amino acid residues (IVGG and ITP, Figure 1(a)), and exhibit

relatively high levels of catalytic activity. The difference in catalytic activity between the two subfamilies reaches up to five orders of magnitude. We reasoned that installing the longer loops from RC-RNase onto ONC could enhance its catalytic activity. Accordingly, two ONC variants (IVGG/ITP and L27I/F28Y/IVGG/ITP ONC) were designed and tested for their ribonucleolytic activity. The L27I/F28Y substitutions were added to mimic the loop structure of RC-RNase more closely. These variants did not, however, exhibit increased catalytic activity.

Local approach

A conspicuous feature of the ONC–d(AUGA) complex was the absence of significant electron density for the two flanking adenosine nucleosides in the nucleic acid (Figure 1(b)). This lack of electron density suggests a negligible interaction of these nucleosides with the enzyme. We asked whether the incorporation of residues that would promote "local" interaction with substrate could revive the catalytic activity of ONC. In RNase A, residues denoted as P subsites participate in substrate binding. These P-subsite residues are cationic lysine or arginine residues that can promote binding with the anionic phosphoryl groups in the nucleic acid backbone through favorable Coulombic interaction.[44] Removal of any residue from the P subsites leads to a loss in catalytic activity and substrate binding.[53,46] In the ONC–d(AUGA) complex structure, no residue other than the active-site lysine residues (Lys9 and Lys31; P_1 subsite, Figure 1(d)), interacts with phosphoryl groups in the nucleic acid. We hypothesized that installing a novel P subsite in ONC would increase its catalytic activity by enhancing substrate binding. A detailed structural comparison between the RNase A–d(ATAAG) complex (PDB entry 1RCN) and the ONC complex pointed towards Thr5 in ONC as being a promising location for a novel P subsite.[44] Consequently, we created the T5K and T5R variants and measured their catalytic activity. In this regard, the T5R substitution performed better than the T5K substitution, conferring a twofold increase in catalytic activity.

Val37 in RC-RNase is involved in nucleobase recognition (B_1 subsite).[52] The corresponding residue in ONC is Lys33. K33V ONC was designed to test whether this substitution could increase nucleobase recognition in ONC. The catalytic activity of K33V ONC did not, however, differ from that of wild-type ONC.

Catalytic activity toward GpG

Excess wild-type ONC (10 μM) did not catalyze the cleavage of 6-FAM–dUrGdGdA–6-TAMRA or 6-FAM–dArGdGdA–6-TAMRA with a rate measurable by our assay. We estimate the values of k_{cat}/K_M to be <1.0 M^{-1} s^{-1}. As a positive control, we used RNase T$_1$, which cleaves RNA at the 3′-side of guanosine residues.[54] One unit of RNase T$_1$ (which produces an increase of 0.0004 A_{260} unit in 1 min in

Table 3. Values of K_i for ONC and its variants

ONC	K_i (μM)	
	5′-GMP	5′-AMP
Wild-type	$6.7(\pm 0.5) \times 10^2$	$3.7(\pm 0.3) \times 10^3$
T89K	$5.3(\pm 0.2) \times 10^2$	$2.0(\pm 0.2) \times 10^3$
T89R	$4.3(\pm 0.6) \times 10^2$	$2.4(\pm 0.4) \times 10^3$
T89N	$1.0(\pm 0.1) \times 10^3$	$1.2(\pm 0.1) \times 10^3$
E91A	$1.3(\pm 0.3) \times 10^3$	$3.2(\pm 0.4) \times 10^3$
T89N/E91A	$9.9(\pm 0.7) \times 10^2$	$5.9(\pm 0.2) \times 10^2$

Values of K_i ($\pm$SE) are for inhibition of catalysis of 6-FAM–dArUdGdA–6-TAMRA cleavage in 0.10 M Mes–NaOH (pH 6.0), 0.10 M NaCl at 23($\pm$2) °C.

1 ml at room temperature using GpA as substrate) catalyzed the cleavage of our two GpG substrates to completion within a minute (data not shown).

Cytotoxicity of ONC variants

All ONC variants with altered nucleobase preference were less toxic than the wild-type enzyme for K-562 cells (Table 2). Likewise, ONC variants designed to possess increased catalytic activity displayed less cytotoxic activity than did wild-type ONC.

Discussion

Molecular basis for the *B₂*-subsite specificity of ONC

The contribution hydrogen bonds in an enzyme–substrate interface to catalysis has been established.[55–59] In the structure of an ONC–nucleic acid complex, $O^{\varepsilon 1}$ and $O^{\varepsilon 2}$ of Glu91 form two hydrogen bonds with $N_{(1)}$ and $N_{(2)}$ of the guanine nucleobase (Figure 1(d)). In addition, Thr89 is located proximal to the guanine nucleobase. The distances between $O^{\gamma 1}$ and $C^{\gamma 2}$ of Thr89, and $O_{(6)}$ of guanine are 3.57 Å and 4.25 Å, respectively. Similar interactions were observed in the RC-RNase·d (ACGA) complex.[52] Specifically, Lys95 and Glu97 from RC-RNase establish an extensive network of hydrogen bonds with the nucleobase. Replacement of these residues with alanine resulted in a significant change in nucleobase preference.[52] To understand the molecular basis underlying the nucleobase specificity of ONC, we took a more systematic approach; we replaced Thr89 and Glu91 with residues that vary in their ability to form hydrogen bonds or in their net charge (or both).

Catalysis of UpG cleavage by wild-type ONC is 110-fold more efficient than is the cleavage of UpA (Table 2). Each of the substitutions made at position 91 (alanine, glutamine, asparagine, and lysine) necessarily led to the loss of the two Glu91–guanine hydrogen bonds observed in the crystalline complex (Figure 1(d)); and each of these variants exhibited a lower preference for guanine. The lysine substitution had the largest effect, actually producing a slight preference for adenine. It is worth noting that this specificity change originates from both a decrease in the catalytic activity toward the UpG substrate and an increase toward the UpA substrate.

To understand the substrate specificity on ONC in greater detail, we performed electrostatic potential calculations. The results are in agreement with previous calculations,[60] showing that the electron density on $N_{(1)}$ and $N_{(2)}$ of guanine is low (Figure 5). Thus, the interaction of this region with the anionic side-chain of Glu91 would be promoted by favorable Coulombic interaction. The electrostatic potential of adenine differs significantly from that of guanine. The electron density on the corresponding
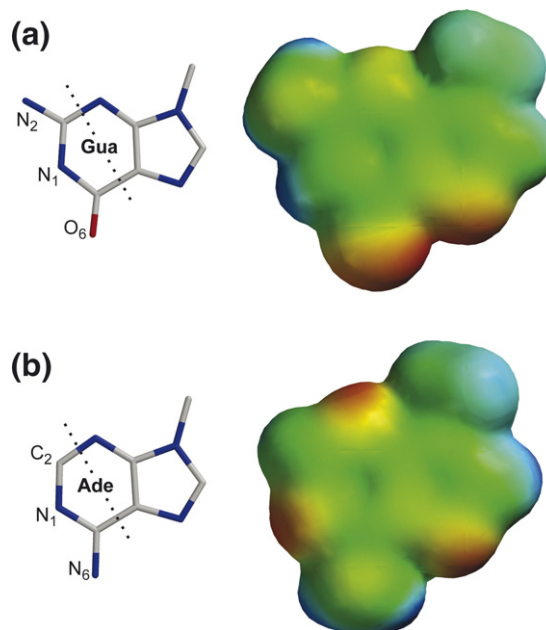

Figure 5. Structure and electron density diagram of (a) 9-methylguanine and (b) 9-methyladenine. Atoms to the left of the broken lines interact with Thr89 and Glu91 of the B₂ subsite of ONC (Figure 1(d)). The electron density of the nucleobases was calculated with the program SPARTAN (Wavefunction, Irvine, CA). Electron-rich regions are colored red; electron-poor regions are colored blue; neutral regions are colored green.

region of adenine is high, and the anionic side-chain of Glu91 would produce unfavorable interactions. We conclude that the 110-fold preference of ONC for a guanine nucleobase can be explained, at least in part, by electrostatic interactions between Glu91 and a purine nucleobase.

The structure of the ONC–d(AUGA) complex predicts that $O_{(6)}$ of the guanine nucleobase would be located close to a cationic side-chain at position 89. In the RC-RNase–d(ACGA) complex, a lysine residue at the corresponding position makes a hydrogen bond with $O_{(6)}$ of guanine.[52] Our data demonstrate that a residue bearing a positive charge at this position (lysine or arginine) strengthens the guanine preference of ONC, while a negative charge (aspartate) attenuates that preference. Because $O_{(6)}$ on guanine is electron-rich, and $N_{(6)}$ on adenine is electron-poor (Figure 2), this result suggests again that the substrate specificity of ONC originates from its electrostatic interaction with the nucleobases. It is not clear, however, why T89N ONC has increased catalytic activity for the UpA substrate, because this substitution does not involve a change in net charge. We have also shown that the increase in catalytic activity toward the UpA substrate by the single substitutions can be enhanced further by their combination. T89N/E91A ONC, a variant that would possess two compatible interfaces for adenine, displays an 11-fold enhanced catalytic activity toward the UpA substrate. Furthermore, this double variant now prefers adenine to guanine by 2.6-fold.

We used the inhibitory effect of 5′-GMP or 5′-AMP on the cleavage of 6-FAM–dArUdGdA–6-TAMRA to assess the effect of substitutions on ground-state binding (Table 2). In this analysis, we assume that the mononucleotides bind at the B_2 and P_1 subsites, and that this binding competitively inhibits the cleavage of the substrate. The inhibitory effect of 5′-AMP is somewhat enhanced in T89K ONC and T89R ONC, indicating that binding of adenine at the B_2 subsite is slightly stronger in these variants, despite the adverse Coulombic effect of adding a positive charge. The binding of guanine became only slightly stronger after the substitutions. Thus, the major ramification of the extra positive charge at position 89 is the destabilization of transition-state binding of adenine, as shown in the considerably decreased k_{cat}/K_M values (Table 2). The T89N substitution lowers the ground-state energy of the enzyme–adenine complex as indicated by the three-fold lower value of K_i. The E91A substitution destabilizes the ground-state binding of guanine.

Guanine and adenine are part of nucleotides with a broad range of distinct biological functions. Discrimination between these two nucleobases, similar in shape and size, is critical for many enzymes (e.g. kinases, ATPases, and GTPases). These proteins usually exhibit a strong preference for their cognate nucleotide over the other. Statistical analyses of protein–nucleotide structures in the RCSB Protein Data Bank has suggested that Coulombic interactions and a network of hydrogen bonds are the two major determinants of selectivity.[61,60] A hydrogen bond is primarily an electrostatic interaction,[62] and a correlation between hydrogen bonds and the electrostatic potential distribution in the protein–ligand interface was indeed found in the statistical analyses. In accord with these findings, our study indicates that Glu91 of ONC uses both Coulombic interactions and hydrogen bonds to confer nucleobase specificity.

Rational design of ONC with enhanced catalytic activity

Implanting extra amino acid residues (IVGG and ITP) designed to affect the "global" breathing motion on ONC did not increase its catalytic activity (Table 2).[49] This result implies that the factors causing the low level of catalytic activity of ONC reside outside the loops. The greater catalytic activity and flexibility attained by the M23L substitution supports this notion.[9,47,49] Met23 is located in a hydrophobic cavity created by the side-chains of Ile22, Phe28, Lys31, Phe36, Cys68, and Tyr77. A bulky leucine residue at this position is thought to alter the position of residues that are critical for catalysis, especially that of Lys31. In this regard, it would be interesting to identify the amino acid residues responsible for rigidity in the β-sheet region by thorough sequence and structural comparison of amphibian ribonucleases. The "local" modifications (T5K, T5R, and K33V substitutions) did not result in a sizeable increase in catalytic acti-

vity. It is possible that the envisioned local interactions were not realized due to the low level of flexibility of ONC.

It is noteworthy that His97 in the ONC–d(AUGA) complex assumes a conformation distinct from that of corresponding histidine residues in other members of the RNase A superfamily. His97 is thought to function as an acid during catalysis by ONC (Figure 2), providing a proton to the displaced $O^{5'}$. In the RNase A–d(ATAAG) and RC-RNase–d(ACGA) complexes, the corresponding histidine residue adopts a suitable conformation for the transfer of a proton from $N^{\delta1}$ to $O^{5'}$.[44,52] The distance between $N^{\delta1}$ and $O^{5'}$ is 2.99 Å and 3.01 Å in the RNase A–d(ATAAG) and RC-RNase–d(ACGA) complex, respectively. In the ONC–d(AUGA) complex, however, the imidazole ring of His97 is rotated by nearly 180° about the χ_2 dihedral angle, such that the $N^{\delta1}$–$O^{5'}$ distance is 5.35 Å (Figure 1(d)). In addition, $N^{\delta1}$ forms a hydrogen bond with $O^{\gamma1}$ of Thr89, which is not conserved in either RNase A or RC-RNase. Thus in ONC, $N^{\epsilon2}$ of His97 rather than $N^{\delta1}$ could be the proton source.

Under physiological conditions, His97 could adopt a more conventional conformation. Twenty-five years ago, the corresponding histidine residue in RNase A was refined in two alternative conformations, indicative of its intrinsic flexibility.[63,64] This histidine residue in RC-RNase exhibits conformational flexibility upon ligand binding.[52] Likewise, the χ_1 dihedral angle of His97 differs by nearly 180° in unliganded ONC (PDB entry 1ONC) and the ONC–d(AUGA) complex. Regardless of this apparent flexibility, both His10 and His97 appear to participate in the catalysis of RNA cleavage (Figure 2), as the pH *versus* k_{cat}/K_M profile of ONC retains the bell shape that is characteristic for the RNase A superfamily (Figure 3),[35–37] and is known to arise from the titration of the two active-site histidine residues.[65]

In vivo cleavage sites for ONC

tRNA has been shown to be a predominant cellular target for ONC.[29] However, it remains a matter of debate whether cellular tRNA is the sole substrate for ONC in the cell.[66] Members of the RNase A superfamily usually cleave a single-stranded region of RNA that is not base-paired. How tRNA, which is extensively base-paired, becomes a target for ONC is unknown. Moreover, calculations predict that most of the tRNA in mammalian mitochondria and *Escherichia coli* exists as a ternary complex with elongation factor Tu (EF-Tu) and GTP,[67] which would limit accessibility to ONC even further. A recent report shed some light on this issue. Through an extensive sequence analysis of the cleavage site in tRNA, Suhasini & Sirdeshimukh demonstrated that ONC preferentially targets the variable loop or the D-arm in tRNA.[30] These regions of tRNA lack base-pairing and are thus candidates for cleavage by ONC. In our ONC–d(AUGA) structure, ONC makes minimal con-

tacts with substrate (only one *P* and two *B* subsites), implying that a compact single-stranded region in RNA is sufficient for an ONC substrate. In addition, the structure of the EF-Tu–GMP–tRNA^{Phe} complex (PDB entry 1TTT)[68] confirms that the variable loop and the D-arm regions are not blocked by EF-Tu. Remarkably, the authors found that the predominant cleavage site is a guanosine–guanosine phosphodiester bond. In the structure of the ONC–d(AUGA) complex, the narrow B_1 subsite composed of Lys33, Thr35, and Phe98 makes intimate contact with the small uracil nucleobase (Figure 1(d)), and would likely occlude the large guanine nucleobase. To determine whether ONC catalyzes the cleavage of a guanosine–guanosine phosphodiester bond *in vitro*, we developed two novel substrates (6-FAM–dUrGdGdA–6-TAMRA and 6-FAM–dArGdGdA–6-TAMRA). The inability of ONC to cleave either substrate leads us to conclude that the B_1 subsite of ONC is too constricted to accommodate a large guanine nucleobase in an unstructured RNA molecule, at least in its *anti* orientation. We conclude that unidentified elements of tRNA structure are involved in the cleavage of the guanosine–guanosine phosphodiester bond in tRNA.

Conclusions

We have determined the crystalline structure of two ONC–nucleic acid complexes at a resolution of 1.90 Å and 1.65 Å. Guided by these structures, we have revealed the atomic basis for substrate recognition and turnover by ONC. We have discovered that ONC utilizes Coulombic interactions (especially from Glu91) and a hydrogen bonding network to mediate substrate specificity, and have demonstrated that rational amino acid substitutions can alter this specificity. Finally, we have probed structural attributes responsible for the low catalytic activity of ONC and the unusual cleavage of a guanosine–guanosine phosphodiester bond in tRNA.

Materials and Methods

Materials

Human RI (RNasin®) was from Promega (Madison, WI). RNase T$_1$ was from Ambion (Austin, TX). 6-Carboxyfluorescein–dArUdAdA–6-carboxytetramethylrhodamine (6-FAM–dArUdAdA–6-TAMRA), 6-FAM–dArUdGdA–6-TAMRA, 6-FAM–dUrGdGdA–6-TAMRA, and 6-FAM–dArGdGdA–6-TAMRA were from Integrated DNA Technologies (Coralville, IA). Mes, 5'-AMP, and 5'-GMP were from Sigma Chemical (St. Louis, MO). Mes was purified further by anion-exchange chromatography to eliminate contaminating oligo(vinylsulfonic acid), which is a potent inhibitor of ribonucleases.[69] The [*methyl*-^{3}H] thymidine was from PerkinElmer Life Sciences (Boston, MA). Phosphate-buffered saline (PBS) contained in 1 liter, 0.20 g of KCl, 0.20 g of KH$_2$PO$_4$, 8.0 g of NaCl, and 2.16 g of Na$_2$HPO$_4$.7H$_2$O. All other chemicals and reagents were of commercial grade or better, and were used without further purification.

K-562 cells, which derive from a continuous human chronic myelogenous leukemia line, were from the American Type Culture Collection (Manassas, VA). Cell culture medium and supplements were from Invitrogen (Carlsbad, CA).

Biophysical measurements

Mass was measured by matrix-assisted laser desorption/ionization–time-of-flight (MALDI–TOF) mass spectrometry using a Voyager-DE-PRO Biospectrometry Workstation Applied Biosystems, Foster City, CA) and a 3,5-dimethoxy-4-hydroxycinnamic acid (sinapinic acid) matrix (Sigma Chemical). Fluorescence measurements were performed with a QuantaMaster 1 photon counting fluorimeter equipped with sample stirring (Photon Technology International, South Brunswick, NJ). Radioactivity was quantified with a Microbeta TriLux liquid scintillation and luminescence counter (PerkinElmer, Wellesley, MA).

Production of ONC and its variants

Wild-type ONC and its variants were produced in *E. coli* strain BL21(DE3) as described.[21] The observed molecular mass of each purified protein was within 0.1% of its expected molecular mass (Table 2). The yield of each purified protein was ≥20 mg per liter of culture.

Crystal preparation

Crystals of T89N/E91A ONC were grown at 20 °C by the hanging-drop method from a solution containing 21.4 mg/ml of protein in water mixed with an equivalent volume of reservoir solution, which was 90 mM bis-Tris buffer (pH 6.5), containing 30.6% (w/v) polyethylene glycol monomethyl ether 2000 and 50 mM 5'-AMP. Crystals were soaked in a reservoir solution supplemented with 5% (v/v) ethylene glycol and then flash-frozen in a stream of nitrogen gas.

Crystals of the wild-type ONC–d(AUGA) complex were grown at 20 °C by the hanging-drop method from a solution containing 10 mg/ml of protein and 3.0 mM nucleic acid in water mixed with an equivalent volume of reservoir solution (0.10 M Hepes (pH 7.5), 25% (v/v) polyethylene glycol (PEG) 3350. Crystals were soaked in reservoir solutions supplemented with increasing amounts of ethylene glycol (up to 20%, v/v), and then flash-frozen in a stream of nitrogen gas.

X-ray data collection

X-ray diffraction data for the T89N/E91A ONC–5'-AMP and the wild-type ONC–d(AUGA) complex were collected with a Bruker AXS Proteum R CCD detector and Microstar rotating-anode generator using copper K$_\alpha$ radiation. All data were processed and scaled with the programs SAINT and SADABS from the Proteum software suite (Bruker, Madison, WI).

Structure refinement

The structures of the T89N/E91A ONC–5'-AMP and the wild-type ONC–d(AUGA) complex were solved by

molecular replacement with apo-ONC (PDB entry 1ONC)[4] as a model using the program MOLREP.[70] The structures were completed using alternate cycles of manual building in Coot,[71] and refinement in REFMAC5.[72] The stereochemical quality of the final models was assessed with MolProbity.[73]

Assays of catalytic activity

The ribonucleolytic activity of wild-type ONC and its variants was measured with a hypersensitive assay based on the cessation of fluorescence quenching as described.[21] To assess the B_2-subsite specificity of ONC, two fluorogenic substrates that contain distinct nucleobase sequences were used. Preference for interaction with the guanine nucleobase was measured by using 6-FAM–dArUdGdA–6-TAMRA, and the interaction with the adenine nucleobase was measured by using 6-FAM–dArUdAdA–6-TAMRA. We also assessed the catalytic activity of wild-type ONC toward two novel ONC substrates, each containing a single cleavable guanosine–guanosine phosphodiester bond: 6-FAM–dUrGdGdA–6-TAMRA and 6-FAM–dArGdGdA–6-TAMRA.

pH *versus* k_{cat}/K_M profile

The effect of pH on the value of k_{cat}/K_M for the cleavage of 6-FAM–dArUdGdA–6-TAMRA by wild-type ONC was determined in 2.00 ml of buffer, 1.0 M NaCl, 6-FAM–dArUdGdA–6-TAMRA (50–500 nM), and wild-type ONC (50 nM–1.0 μM). The 1.0 mM buffers were: sodium formate–HCl (pH 4.07); sodium acetate–HCl (pH 4.43–5.54); bis-Tris–NaOH (pH 6.0–6.64); Mops–NaOH (pH 7.09–7.43); and Tris–HCl (pH 7.87). The pH values of the buffers were determined with a Φ40 pH meter from Beckman Instruments (Fullerton, CA). The concentration of buffer was kept low to ensure an identical salt environment, which is known to affect catalysis by ribonucleases.[53,75] No change in the pH value of reaction mixtures was detectable during the course of the reaction. A higher concentration of he substrate (350–500 nM) was used at acidic pH than the 50 nM concentration used at basic pH, because the protonation of the fluorescein moiety of the substrate decreases its fluorescence intensity. To obtain values of K_1 and K_2, which are the apparent macroscopic acid dissociation constants of two functional groups important in catalysis, data were fit by non-linear, least-squares regression analysis with the program PRISM 4 (GraphPad Software, San Diego, CA) to equation (1):

$$k_{cat}/K_M = \frac{(k_{cat}/K_M)_{max}}{\dfrac{[H^+]}{K_1} + 1 + \dfrac{K_2}{[H^+]}} \qquad (1)$$

where $(k_{cat}/K_M)_{max}$ is the pH-independent specificity constant.

Inhibition of catalytic activity

Inhibition of ribonucleolytic activity was measured using 6-FAM–dArUdGdA–TAMRA as a substrate. Inhibition by 5′-AMP or 5′-GMP was assessed at 25 °C in 2.0 ml of 50 mM imidazole–HCl buffer (pH 6.0) containing 0–0.25 M NaCl, 60 nM 6-FAM–dArUdAdA–6-TAMRA, and 1–5 nM ONC as described.[76,77] We assumed that the nucleobases of 5′-AMP and 5′-GMP bind exclusively at the B_2 subsite, because the narrow B_1 subsite cannot accommodate a purine. This assumption is supported by our finding that ONC does not cleave our novel substrates containing a guanosine–guanosine phosphodiester bond (*vide supra*).

In the crystalline T89N/E91A ONC–5′-AMP complex, four 5′-AMP molecules are bound in a mode that is not productive, in that the active site is occupied by phosphoryl groups from two 5′-AMP molecules and no adenine nucleobase is proximal to the B_2 subsite (i.e. Asn89 and Ala91). The formation of such a non-productive complex is unlikely during our inhibition assay. The 5′-AMP molecules in the crystalline T89N/E91A ONC–5′-AMP complex are shared by multiple enzyme molecules in the crystal lattice, which is comprised of an extensive array of enzymes and nucleotides. Such protein–nucleotide interactions are unlikely to form in dilute aqueous solution.

Fluorescence (*F*) was measured with 493 nm and 515 nm as the excitation and emission wavelengths, respectively. The value of $\Delta F/\Delta t$ was measured for 3 min after the addition of ONC. Next, an aliquot of inhibitor (I) dissolved in the assay buffer was added, and $\Delta F/\Delta t$ was measured in the presence of the inhibitor for 3 min. The concentration of inhibitor in the assay was doubled repeatedly at 3 min intervals. Excess wild-type RNase A was then added to the mixture to ensure that <10% of the substrate had been cleaved before completion of the inhibition assay. Apparent changes in ribonucleolytic activity due to dilution were corrected by comparing values to those from an assay in which aliquots of buffer were added. To obtain values of K_i, data were fit by non-linear, least-squares regression analysis with the program DELTA-GRAPH 5.5 (Red Rock Software, Salt Lake City, UT) to equation (2):[76,77]

$$\Delta F/\Delta t = (\Delta F/\Delta t)_0 \left(\frac{K_i}{[I] + K_i} \right) \qquad (2)$$

where $(\Delta F/\Delta t)_0$ is the ribonucleolytic activity before the addition of the inhibitor.

Assays of cytotoxic activity

The effect of wild-type ONC, its variants, and RNase A on cell proliferation was determined as described.[21] Cytotoxicity data were analyzed with the programs SIGMAPLOT (SPSS Science, Chicago, IL) and DELTA-GRAPH 5.5. Each datum point represents the mean (±SE) of at least three experiments performed in triplicate. To obtain values of IC$_{50}$, data were fit by non-linear, least squares regression analysis with the program DELTA-GRAPH 5.5 to equation (3):[78]

$$S = \frac{IC_{50}}{IC_{50} + [ribonuclease]} \times 100 \qquad (3)$$

where S is the percentage of total DNA synthesis during the 4 h pulse as compared to that of a PBS control.

Protein Data Bank accession numbers

The final coordinates have been deposited in the RCSB Protein Data Bank[74] with accession numbers 2GMK and 2I5S for the T89N/E91A ONC–5′-AMP and wild-type ONC–d(AUGA) complexes, respectively.

Acknowledgements

References

1. Leland, P. A. & Raines, R. T. (2001). Cancer chemotherapy – ribonucleases to the rescue. *Chem. Biol.* **8**, 405–413.

2. Tafech, A., Bassett, T., Sparanese, D. & Lee, C. H. (2006). Destroying RNA as a therapeutic approach. *Curr. Med. Chem.* **13**, 863–881.

3. Raines, R. T. (1998). Ribonuclease A. *Chem. Rev.* **98**, 1045–1065.

4. Mosimann, S. C., Ardelt, W. & James, M. N. G. (1994). Refined 1.7 Å X-ray crystallographic structure of P-30 protein, an amphibian ribonuclease with anti-tumor activity. *J. Mol. Biol.* **236**, 1141–1153.

5. Mikulski, S. M., Costanzi, J. J., Vogelzang, N. J., McCachren, S., Taub, R. N., Chun, H. *et al.* (2002). Phase II trial of a single weekly intravenous dose of ranpirnase in patients with unresectable malignant mesothelioma. *J. Clin. Oncol.* **20**, 274–281.

6. Pavlakis, N. & Vogelzang, N. J. (2006). Ranpirnase— an antitumour ribonuclease: its potential role in malignant mesothelioma. *Expert Opin. Biol. Ther.* **6**, 391–399.

7. Youle, R. J., Wu, Y. N., Mikulski, S. M., Shogen, K., Hamilton, R. S., Newton, D. *et al.* (1994). RNase inhibition of human immunodeficiency virus infection of H9 cells. *Proc. Natl Acad. Sci. USA*, **91**, 6012–6016.

8. Leland, P. A., Staniszewski, K. E., Kim, B. & Raines, R. T. (2000). A synapomorphic disulfide bond is critical for the conformational stability and cytotoxicity of an amphibian ribonuclease. *FEBS Letters*, **477**, 203–207.

9. Notomista, E., Catanzano, F., Graziano, G., Dal Piaz, F., Barone, G., D'Alessio, G. & Di Donato, A. (2000). Onconase: an unusually stable protein. *Biochemistry*, **39**, 8711–8718.

10. Notomista, E., Catanzano, F., Graziano, G., Di Gaetano, S., Barone, G. & Di Donato, A. (2001). Contribution of chain termini to the conformational stability and biological activity of onconase. *Biochemistry*, **40**, 9097–9103.

11. Arnold, U., Schulenburg, C., Schmidt, D. & Ulbrich-Hofmann, R. (2006). Contribution of structural peculiarities of onconase to its high stability and folding kinetics. *Biochemistry*, **45**, 3580–3587.

12. Dickson, K. A., Haigis, M. C. & Raines, R. T. (2005). Ribonuclease inhibitor: Structure and function. *Prog. Nucl. Acid Res. Mol. Biol.* **80**, 349–374.

13. Lee, F. S., Shapiro, R. & Vallee, B. L. (1989). Tight-binding inhibition of angiogenin and ribonuclease A by placental ribonuclease inhibitor. *Biochemistry*, **28**, 225–230.

14. Lee, F. S. & Vallee, B. L. (1989). Binding of placental ribonuclease inhibitor to the active site of angiogenin. *Biochemistry*, **28**, 3556–3561.

15. Vicentini, A. M., Kieffer, B., Matthies, R., Meyhack, B., Hemmings, B. A., Stone, S. R. & Hofsteenge, J. (1990). Protein chemical and kinetic characterization of recombinant porcine ribonuclease inhibitor expressed in *Saccharomyces cerevisiae*. *Biochemistry*, **29**, 8827–8834.

16. Shapiro, R. & Vallee, B. L. (1991). Interaction of human placental ribonuclease with placental ribonuclease inhibitor. *Biochemistry*, **30**, 2246–2255.

17. Boix, E., Wu, Y., Vasandani, V. M., Saxena, S. K., Ardelt, W., Ladner, J. & Youle, R. J. (1996). Role of the N terminus in RNase A homologues: differences in catalytic activity, ribonuclease inhibitor interaction and cytotoxicity. *J. Mol. Biol.* **257**, 992–1007.

18. Haigis, M. C., Kurten, E. L. & Raines, R. T. (2003). Ribonuclease inhibitor as an intracellular sentry. *Nucl. Acids Res.* **31**, 1024–1032.

19. Johnson, R. J., McCoy, J. G., Bingman, C. A., Phillips, G. N., Jr & Raines, R. T. (2007). Inhibition of human pancreatic ribonuclease by the human ribonuclease inhibitor protein. *J. Mol. Biol.* **368**, 434–449.

20. Dickson, K. A., Dahlberg, C. L. & Raines, R. T. (2003). Compensating effects on the cytotoxicity of ribonuclease A variants. *Arch. Biochem. Biophys.* **415**, 172–177.

21. Lee, J. E. & Raines, R. T. (2003). Contribution of active-site residues to the function of onconase, a ribonuclease with antitumoral activity. *Biochemistry*, **42**, 11443–11450.

22. Wu, Y., Mikulski, S. M., Ardelt, W., Rybak, S. M. & Youle, R. J. (1993). A cytotoxic ribonuclease. Study of the mechanism of onconase cytotoxicity. *J. Biol. Chem.* **268**, 10686–10693.

23. Rushizky, G. W., Knight, C. A. & Sober, H. A. (1961). Studies on the preferential specificity of pancreatic ribonuclease as deduced from partial digests. *J. Biol. Chem.* **236**, 2732–2737.

24. Wlodawer, A., Miller, M. & Sjolin, L. (1983). Active site of RNase: neutron diffraction study of a complex with uridine vanadate, a transition-state analog. *Proc. Natl Acad. Sci. USA*, **80**, 3628–3631.

25. delCardayré, S. B. & Raines, R. T. (1994). Structural determinants of enzymatic processivity. *Biochemistry*, **33**, 6031–6037.

26. Kelemen, B. R., Schultz, L. W., Sweeney, R. Y. & Raines, R. T. (2000). Excavating an active site: the nucleobase specificity of ribonuclease A. *Biochemistry*, **39**, 14487–14494.

27. Okabe, Y., Katayama, N., Iwama, M., Watanabe, H., Ohgi, K., Irie, M. *et al.* (1991). Comparative base specificity, stability, and lectin activity of two lectins from eggs of *Rana catesbeiana* and *R. japonica* and liver ribonuclease from *R. catesbeiana*. *J. Biochem. (Tokyo)*, **109**, 786–790.

28. Witzel, H. & Barnard, E. A. (1962). Mechanism and binding sites in the ribonuclease reaction. II. Kinetic studies on the first step of the reaction. *Biochem. Biophys. Res. Commun.* **7**, 295–299.

29. Saxena, S. K., Sirdeshmukh, R., Ardelt, W., Mikulski, S. M., Shogen, K. & Youle, R. J. (2002). Entry into cells and selective degradation of tRNAs by a cytotoxic member of the RNase A family. *J. Biol. Chem.* **277**, 15142–15146.

30. Suhasini, A. N. & Sirdeshmukh, R. (2006). Transfer RNA cleavages by onconase reveal unusual cleavage sites. *J. Biol. Chem.* **281**, 12201–12209.

31. Findlay, D., Herries, D. G., Mathias, A. P., Rabin, B. R. & Ross, C. A. (1961). The active site and mechanism of action of bovine pancreatic ribonuclease. *Nature*, **190**, 781–784.

32. Findlay, D., Herries, D. G., Mathias, A. P., Rabin, B. R. & Ross, C. A. (1962). The active site and mechanism of action of bovine pancreatic ribonuclease. 7. The catalytic mechanism. *Biochem. J.* **85**, 152–153.

33. Roberts, G. C., Dennis, E. A., Meadows, D. H., Cohen, J. S. & Jardetzky, O. (1969). The mechanism of action of ribonuclease. *Proc. Natl Acad. Sci. USA*, **62**, 1151–1158.

34. Thompson, J. E., Venegas, F. D. & Raines, R. T. (1994). Energetics of catalysis by ribonucleases: fate of the 2′,3′-cyclic phosphodiester intermediate. *Biochemistry*, **33**, 7408–7414.

35. Herries, D. G., Mathias, A. P. & Rabin, B. R. (1962). The active site and mechanism of action of bovine pancreatic ribonuclease. 3. The pH-dependence of the kinetic parameters for the hydrolysis of cytidine 2′,3′-phosphate. *Biochem. J.* **85**, 127–134.

36. del Rosario, E. J. & Hammes, G. G. (1969). Kinetic and equilibrium studies of the ribonuclease-catalyzed hydrolysis of uridine 2′,3′-cyclic phosphate. *Biochemistry*, **8**, 1884–1889.

37. Lou, Y. C., Huang, Y. C., Pan, Y. R., Chen, C. & Liao, Y. D. (2006). Roles of *N*-terminal pyroglutamate in maintaining structural integrity and pK_a values of catalytic histidine residues in bullfrog ribonuclease 3. *J. Mol. Biol.* **355**, 409–421.

38. Liao, Y. D., Huang, H. C., Leu, Y. J., Wei, C. W., Tang, P. C. & Wang, S. C. (2000). Purification and cloning of cytotoxic ribonucleases from *Rana catesbeiana* (bullfrog). *Nucl. Acids Res.* **28**, 4097–4104.

39. Markley, J. L. (1975). Correlation proton magnetic resonance studies at 250 MHz of bovine pancreatic ribonuclease. I. Reinvestigation of the histidine peak assignment. *Biochemistry*, **14**, 3546–3553.

40. Quirk, D. J. & Raines, R. T. (1999). His···Asp catalytic dyad of ribonuclease A: Histidine pK_a values in the wild-type, D121N, and D121A enzymes. *Biophys. J.* **76**, 1571–1579.

41. Park, C., Schultz, L. W. & Raines, R. T. (2001). Contribution of the active site histidine residues of ribonuclease A to nucleic acid binding. *Biochemistry*, **40**, 4949–4956.

42. Tarragona-Fiol, A., Eggelte, H. J., Harbron, S., Sanchez, E., Taylorson, C. J., Ward, J. M. & Rabin, B. R. (1993). Identification by site-directed mutagenesis of amino acids in the B2 subsite of bovine pancreatic ribonuclease A. *Protein Eng.* **6**, 901–906.

43. delCardayré, S. B. & Raines, R. T. (1995). A residue to residue hydrogen bond mediates the nucleotide specificity of ribonuclease A. *J. Mol. Biol.* **252**, 328–336.

44. Fontecilla-Camps, J. C., de Llorens, R., le Du, M. H. & Cuchillo, C. M. (1994). Crystal structure of ribonuclease A·d(ApTpApApG) complex. *J. Biol. Chem.* **269**, 21526–21531.

45. Nogués, M. V., Moussaoui, M., Boix, E., Vilanova, M., Ribó, M. & Cuchillo, C. M. (1998). The contribution of noncatalytic phosphate-binding subsites to the mechanism of bovine pancreatic ribonuclease A. *Cell. Mol. Life Sci.* **54**, 766–774.

46. Fisher, B. M., Grilley, J. E. & Raines, R. T. (1998). A new remote subsite in ribonuclease A. *J. Biol. Chem.* **273**, 34134–34138.

47. Gorbatyuk, V. Y., Tsai, C. K., Chang, C. F. & Huang, T. H. (2004). Effect of *N*-terminal and Met23 mutations on the structure and dynamics of onconase. *J. Biol. Chem.* **279**, 5772–5780.

48. Shindyalov, I. N. & Bourne, P. E. (1998). Protein structure alignment by incremental combinatorial extension (CE) of the optimal path. *Protein Eng.* **11**, 739–747.

49. Merlino, A., Mazzarella, L., Carannante, A., Di Fiore, A., Di Donato, A., Notomista, E. & Sica, F. (2005). The importance of dynamic effects on the enzyme activity: X-ray structure and molecular dynamics of onconase mutants. *J. Biol. Chem.* **280**, 17953–17960.

50. Rosenberg, H. F., Zhang, J., Liao, Y. D. & Dyer, K. D. (2001). Rapid diversification of RNase A superfamily ribonucleases from the bullfrog, *Rana catesbeiana*. *J. Mol. Evol.* **53**, 31–38.

51. Hsu, C. H., Liao, Y. D., Pan, Y. R., Chen, L. W., Wu, S. H., Leu, Y. J. & Chen, C. (2003). Solution structure of the cytotoxic RNase 4 from oocytes of bullfrog *Rana catesbeiana*. *J. Mol. Biol.* **326**, 1189–1201.

52. Leu, Y. J., Chern, S. S., Wang, S. C., Hsiao, Y. Y., Amiraslanov, I., Liaw, Y. C. & Liao, Y. D. (2003). Residues involved in the catalysis, base specificity, and cytotoxicity of ribonuclease from *Rana catesbeiana* based upon mutagenesis and X-ray crystallography. *J. Biol. Chem.* **278**, 7300–7309.

53. Fisher, B. M., Ha, J.-H. & Raines, R. T. (1998). Coulombic forces in protein–RNA interactions: Binding and cleavage by ribonuclease A and variants at Lys7, Arg10, and Lys66. *Biochemistry*, **37**, 12121–12132.

54. Steyaert, J. (1997). A decade of protein engineering on ribonuclease T1—atomic dissection of the enzyme-substrate interactions. *Eur. J. Biochem.* **247**, 1–11.

55. Carlow, D. C., Short, S. A. & Wolfenden, R. (1998). Complementary truncations of a hydrogen bond to ribose involved in transition-state stabilization by cytidine deaminase. *Biochemistry*, **37**, 1199–1203.

56. Loverix, S., Winqvist, A., Stromberg, R. & Steyaert, J. (2000). Mechanism of RNase T1: Concerted triester-like phosphoryl transfer via a catalytic three-centered hydrogen bond. *Chem. Biol.* **7**, 651–658.

57. Yin, Y., Sampson, N. S., Vrielink, A. & Lario, P. I. (2001). The presence of a hydrogen bond between asparagine 485 and the π system of FAD modulates the redox potential in the reaction catalyzed by cholesterol oxidase. *Biochemistry*, **40**, 13779–13787.

58. Kicska, G. A., Tyler, P. C., Evans, G. B., Furneaux, R. H., Shi, W., Fedorov, A. *et al.* (2002). Atomic dissection of the hydrogen bond network for transition-state analogue binding to purine nucleoside phosphorylase. *Biochemistry*, **41**, 14489–14498.

59. Kim, K. W., Wang, Z., Busby, J., Tsuruda, T., Chen, M., Hale, C. *et al.* (2006). The role of tyrosine 177 in human 11β-hydroxysteroid dehydrogenase type 1 in substrate and inhibitor binding: an unlikely hydrogen bond donor for the substrate. *Biochim. Biophys. Acta*, **1764**, 824–830.

60. Basu, G., Sivanesan, D., Kawabata, T. & Go, N. (2004). Electrostatic potential of nucleotide-free protein is sufficient for discrimination between adenine and guanine-specific binding sites. *J. Mol. Biol.* **342**, 1053–1066.

61. Nobeli, I., Laskowski, R. A., Valdar, W. S. & Thornton, J. M. (2001). On the molecular discrimination between adenine and guanine by proteins. *Nucl. Acids Res.* **29**, 4294–4309.

62. Jeffrey, G. A. (1997). *Introduction to Hydrogen Bonding*, Oxford University Press, New York.

63. Borkakoti, N., Moss, D. S. & Palmer, R. A. (1982). Ribonuclease-A—least-squares refinement of the structure at 1.45 Å resolution. *Acta Crystallog. sect. B*, **38**, 2210–2217.

64. Howlin, B., Moss, D. S. & Harris, G. W. (1989). Segmented anisotropic refinement of bovine ribonuclease-A by the application of the rigid-body TLS model. *Acta Crystallog. sect. A*, **45**, 851–861.

65. Jackson, D. Y., Burnier, J., Quan, C., Stanley, M., Tom, J. & Wells, J. A. (1994). A designed peptide ligase for total synthesis of ribonuclease A with unnatural catalytic residues. *Science*, **266**, 243–247.

66. Ardelt, B., Ardelt, W. & Darzynkiewicz, Z. (2003). Cytotoxic ribonucleases and RNA interference (RNAi). *Cell Cycle*, **2**, 22–24.

67. Cai, Y. C., Bullard, J. M., Thompson, N. L. & Spremulli, L. L. (2000). Interaction of mitochondrial elongation factor Tu with aminoacyl-tRNA and elongation factor Ts. *J. Biol. Chem.* **275**, 20308–20314.

68. Nissen, P., Kjeldgaard, M., Thirup, S., Polekhina, G., Reshetnikova, L., Clark, B. F. C. & Nyborg, J. (1995). Crystal structure of the ternary complex of Phe-tRNA^Phe, EF-Tu, and a GTP analog. *Science*, **270**, 1464–1472.

69. Smith, B. D., Soellner, M. B. & Raines, R. T. (2003). Potent inhibition of ribonuclease A by oligo(vinylsulfonic acid). *J. Biol. Chem.* **278**, 20934–20938.

70. Vagin, A. & Teplyakov, A. (1997). MOLREP: an automated program for molecular replacemet. *J. Appl. Crystallog.* **30**, 1022–1025.

71. Emsley, P. & Cowtan, K. (2004). Coot: model-building tools for molecular graphics. *Acta Crystallog. sect. D*, **60**, 2126–2132.

72. Murshudov, G. N., Vagin, A. A. & Dodson, E. J. (1997). Refinement of macromolecular structures by the maximum-likelihood method. *Acta Crystallog. sect. D*, **53**, 240–255.

73. Lovell, S. C., Davis, I. W., Arendall, W. B., III, de Bakker, P. I. W., Word, J. M., Prisant, M. G. *et al.* (2003). Structure validation by C^α geometry: φ, ψ and C^β deviation. *Proteins: Struct. Funct. Genet.* **50**, 437–450.

74. Berman, H. M., Westbrook, J., Feng, Z., Gilliland, G., Bhat, T. N., Weissig, H. *et al.* (2000). The Protein Data Bank. *Nucl. Acids Res.* **28**, 235–242.

75. Park, C. & Raines, R. T. (2001). Quantitative analysis of the effect of salt concentration on enzymatic catalysis. *J. Am. Chem. Soc.* **123**, 11472–11479.

76. Kelemen, B. R., Klink, T. A., Behlke, M. A., Eubanks, S. R., Leland, P. A. & Raines, R. T. (1999). Hypersensitive substrate for ribonucleases. *Nucl. Acids Res.* **27**, 3696–3701.

77. Park, C., Kelemen, B. R., Klink, T. A., Sweeney, R. Y., Behlke, M. A., Eubanks, S. R. & Raines, R. T. (2001). Fast, facile, hypersensitive assays for ribonucleolytic activity. *Methods Enzymol.* **341**, 81–94.

78. Haigis, M. C., Kurten, E. L., Abel, R. L. & Raines, R. T. (2002). KFERQ sequence in ribonuclease A-mediated cytotoxicity. *J. Biol. Chem.* **277**, 11576–11581.

79. Merritt, E. A. & Murphy, M. E. P. (1994). Raster3D version 2.0: a program for photorealistic molecular graphics. *Acta Crystallog. sect. D*, **50**, 869–873.